Wiley
Journal of Engineering
Volume 2024, Article ID 9085919, 17 pages
https://doi.org/10.1155/2024/9085919

WILEY

Research Article

Deform 3D Simulation and Experimental Study in Machining of AISI 1020 Mild Steel

Aqib Hussain,[1] **Aamer Sharif**,[2] **Muftooh Ur Rehman Siddiqui**,[3] **Ghulam Hussain**,[4] **Melkamu Tadesse Getachew**,[5] **and Riaz Muhammad**[4]

[1]*Department of Mechanical Engineering, CECOS University of IT and Emerging Sciences, Peshawar 25000, Pakistan*
[2]*School of Engineering, Edith Cowan University, Joondalup, Perth, WA 6027, Australia*
[3]*Mechanical, Biomedical and Design Engineering Department, School of Engineering and Technology, Aston University, Birmingham, UK*
[4]*Mechanical Engineering Department, College of Engineering, University of Bahrain, Isa Town Campus, Zallaq, Bahrain*
[5]*Faculty of Mechanical and Industrial Engineering, Bahir Dar Institute of Technology, Bahir Dar University, Bahir Dar, Ethiopia*

Correspondence should be addressed to Melkamu Tadesse Getachew; melkamu19.mt@gmail.com

Received 22 December 2023; Revised 12 April 2024; Accepted 18 May 2024; Published 27 May 2024

Academic Editor: Himadri Majumder

The drilling process plays a crucial role in the assembly process of modern-day manufactories. One of the major causes of component rejection during drilling operations is the incorrect selection of spindle speed and feed rate. Therefore, this study aimed to investigate the impact of process factors such as spindle speed and feed rate on torque, thrust force, temperature surface roughness, and chip formation during the drilling of AISI 1020 mild steel. A combination of finite element modeling and experimental investigation was employed to achieve the process. Specifically, the commercially available finite element software, Deform 3D, was used for simulation. The modeling results were then compared and validated with the experimental data. A high-speed steel drill bit was utilized during the modeling and experimentation. The spindle speed was varied at 330, 410, and 510 rpm, while the feed rates were set at 0.12, 0.2, and 0.3 mm/rev. The study's findings suggest that the spindle speed has an inverse relationship with thrust force, torque, and surface roughness, whereas it has a direct relationship with temperature. Conversely, the feed rate directly correlates with thrust force, torque, temperature, and surface roughness. Additionally, an analysis of the chips produced during the experiments revealed the impact of the cutting conditions on chip formation. The study results showed a 2–10% discrepancy between the experimental and simulation data. The ANOVA results indicated that the feed rate contributes the most to thrust force and torque, with a percentage contribution of 61.73% and 59.87%, respectively, followed by spindle speed, with a percentage contribution of 37.09% and 38.89%, respectively. Furthermore, temperature influences spindle speed the most, followed by feed rate, with percentage contributions of 67.75% and 31.11%, respectively. Moreover, the feed rate's percentage contribution to surface roughness is higher than the spindle speed, with a contribution of 66.20% and 32.18%, respectively.

1. Introduction

In manufacturing, drilling creates a circular hole in a piece of material. Because of its cheap cost and good hole quality, it is an essential tool in machining for assembly activities in automotive and aerospace industries [1–3]. In the automobile industry, it accounts for about 40 percent of all material removal procedures. In contrast, in the aerospace industry, millions of holes are essential in the final assembly of their products [4–6]. A typical aircraft requires nearly 2000 holes only for frame attachment with the main assembly [6, 7]. Improper drilling operations, such as poor drilling conditions and rapid tool wear, can force additional finishing operations and parts rejection, increasing the cost and time of the product [8, 9]. Hence, the desired hole quality can only be achieved by carefully choosing process variables, machine configuration, and cutting equipment [10].

AISI 1020 mild steel has been acknowledged as the most prominent material for all-purpose engineering products such as cams, shafts, ratchet, gudgeon pins, spindles, lightweight gears, and worm gears, as well as other similar items [11]. It is the most widely used low-alloy steel due to its excellent formability and adequate mechanical qualities [12]. High-speed steel (HSS) drill bits are commonly selected in drilling operations because they are more heat-resistant than high-carbon steel [13]. They are challenging and suitable for interrupted cutting and various drilling operations. HSS drill bits are widely used in the metalworking industry to drill high-quality holes in mild steel alloy to achieve high-quality final products. The quality of the drilled holes relies on various machining parameters employed during the fabrication process [14].

Machinability is considered the most prominent factor affecting the alloy's machining performance [15, 16]. Inadequate machinability or poor hole quality can lead to frequent replacement of cutting tools and a decline in machine efficiency [17]. Moreover, incorrect machining parameters can impose undesired thrust forces and torques on the cutting tool, which can cause unwanted deformation in the machined workpiece [18]. The quality of the hole is determined by process parameters, including *n*, *f*, cutting fluid, tool diameter, and chip morphology. It is essential to carefully select process variables to achieve high-quality drilled holes. In particular, *n*, drill tool diameter, and cutting fluid are critical parameters affecting the drilled holes' surface finish. Therefore, the appropriate selection of process variables is imperative to obtain superior-quality drilled holes [19]. The choice of relevant process parameters is crucial to ensure the production of the finest holes [19].

2. Literature Review

Drilling in mild steel has historically been studied using various analytical and experimental methods. It has been shown that even a little discrepancy in the ideal hole shape may dramatically impact the final assembly and lead to the whole item being rejected [20]. Prior research studies have employed various experimental and analytical techniques to improve machinability and drilling performance. Table 1 summarizes some of the investigations conducted in the past on the subject of drilling stainless steel and mild steel.

For instance, Bhole and Shelke [21] investigated the optimum drilling process parameters for AISI 316L following the input parameters such as *f*, *n*, and hole depth affecting the Ra and MRR. The Taguchi method, ANOVA, and linear regression analysis have been utilized to ascertain the control factors that hold the most significance in terms of their effect on Ra and MRR. Sonowal et al. [22] studied the influence of cutting parameters (*f*, *n*, and depth of cut) on Ra using Taguchi and ANOVA in turning AISI 1020 steels. The results show that *f* has a higher influence than *n* and depth of cut on both the mean and variation of Ra in turning AISI 1020 mild steel. Sundeep et al. [28] use the Taguchi L9 array to study austenitic stainless steel drilling (AISI 316) Ra and MRR based on the input parameters, such as the *f*, *n*, and drill diameter results examined that *n* has a more significant influence on Ra and MRR in the drilling process of AISI 316. Kıvak et al. [23] studied the influence of cutting parameters such as *V*, *f* and cutting tools through Taguchi techniques and ANOVA. They concluded that *f* and cutting tools significantly affect Ra and Fz in drilling AISI 316 stainless steel. Siddiquee et al. [19] studied the influence of cutting fluid, hole depth, *f*, and *n* on Ra in the drilling of AISI 312 through ANOVA and Taguchi techniques and concluded that *n* was the dominant element in determining the quality of the finished product. Mahapatra et al. [25] examined the Ra, tool vibration, and chip morphology during the hard turning of AISI H13 steel using a nanofluid mixture of multiwalled carbon nanotubes and minimal lubricant. A statistical analysis reveals that the most significant contribution to Ra comes from nose radius, which accounts for 36.65%, and the highest contribution to tool vibration comes from cutting speed, which accounts for 53.88%. Degradation of machined surface finish is caused by increased tool vibration and flank wear. Segmented type serrated saw-toothed chips were produced during nanofluid-MQL machining. Pradhan et al. [26] addressed the surface and chip morphology when turning a functionally graded (FG) specimen under NFMQL conditions. The outcomes demonstrate that the NFMQL approach produced cleaner, more environmentally friendly, and more sustainable manufacturing. Jena et al. [27] investigated the modeling and optimization of Ra when turning HSLA grade AISI 4340 steel by dry hard turning using a coated ceramic tool. Sixteen sets of experimental data were analyzed using ANOVA, and the results indicated that *f* and *v* are the two most important controlled cutting factors for HT operation in terms of improving surface smoothness. The desirability function analysis of RSM is used to determine the optimum cutting conditions, which aim to minimize Ra.

As per the authors' knowledge, previous literature reveals that there needs to be more research conducted on machining mild steel, especially in drilling AISI 1020 mild steel. Specifically, investigating parameters such as thrust force, torque, temperature, surface roughness, and chip formation under varying *f* and *n* is yet to be explored. Investigating these parameters is essential because of their effect on tool wear and overall machining efficiency. Therefore, characteristics such as thrust force, torque, temperature, surface roughness, and chip formation must be investigated while drilling AISI 1020 mild steel. The thrust force and torque facilitate tool selection and process optimization, which offer information about the forces applied to the cutting tool. In AISI 1020 mild steel machining operations, surface roughness and chip formation analysis assist in achieving desired product quality and dimensional precision. Monitoring temperature prevents overheating, impacting both tool life and material qualities. Moreover, finite element analysis with experimental data needs to be adequately validated.

Therefore, the present study aims to address the above gaps by providing specific insight for achieving efficient material removal and minimizing tool wear by considering the effect of *f* and *n* on torque, thrust force, temperature, chip formation, and Ra, contributing to a comprehensive

Table 1: Summary of previous investigation on drilling steel.

Type	Cutting tool	Cutting parameters	Methods	Output parameters	Year	Reference
AISI 316L	HSS	$n = 1000, 1500, 2000$ rpm $f = 30, 40, 50$ mm/min $H_d = 10, 15, 20$ mm	Taguchi, ANOVA, regression analysis	Ra, MRR	2016	[21]
AISI 1020	M2 HSS	$n = 400, 500, 630$ rpm $f = 0.05, 0.081, 0.113$ min/rev Dc = 0.5, 1.25, 2 mm	Taguchi, ANOVA	Ra	2017	[22]
AISI 316	Twist drill (TiAIN)	$n = 500, 800, 1000$ rpm $f = 0.1, 0.15, 0.2$ mm/rev $d = 6, 8, 10$ mm	ANOVA, Taguchi	Ra, MRR	2012	[23]
AISI 316	M35 HSS twist drill	$v = 12, 14, 16$ m/min $f = 0.1, 0.12$ 0.14 mm/rev	Taguchi, ANOVA	Ra, Fz	2013	[24]
AISI 312	HSS	$n = 300, 400, 500$ rpm $f = 0.03, 0.04, 0.05$ mm/s Hole depth = 25, 30, 35 mm Cutting fluid = absent, present	ANOVA, Taguchi	Ra	2014	[19]
AISI H13 steel	AITiSiN	$d =$, 0.1, 0.2, 0.3 mm $r = 1, 1.2, 1.4$ mm $f = 0.03, 0.07, 0.09$ mm/rev $v = 45$ m/min, 55 m/mm, 65 m/min	Multiresponse optimization, RSM, ANOVA	Ra, flank wear, tool vibration	2023	[25]
FG specimen	Coated carbide tool	$v = 45, 110, 190$ m/min $f = 0.15, 0.25, 0.35$ mm/rev Dc = 0.1, 0.2, 0.3 mm	Taguchi, SEM, RSM, NFMQL	Microstructure, optimal machining limit, surface integrity	2022	[26]
AISI 4340 steel	Coated ceramic tool	$v = 35, 85, 125$ m/min $f = 0.1, 0.2, 0.3$ mm/rev Dc = 0.15, 0.2, 0.3 mm	Taguchi, ANOVA, RSM	Ra	2019	[27]

RSM = response surface methodology, NFMQL = nanofluid-assisted minimal quantity lubrication, HSLA = high-strength low-alloy, SEM = scanning electron microscopy, Dc = depth of cut, H_d = depth of hole, W = tool wear, MRR = material removal rate, Ra = surface roughness, f = feed rate, n = spindle speed, v = cutting speed, d = drill diameter, t = temperature, HSS = high-speed steel, Fz = thrust force, Mz = torque, Af = axial force, θ = point angle, and Ψ = helix angle.

understanding of the machining process for AISI 1020 mild steel. The main objectives of the current study are to compare the simulation results with experimental data focusing on the drilling of AISI 1020 mild steel, specifically on cutting forces and temperature, and validate experimental data with simulation results. The effect of *f* and *n* on Ra and chip formation in AISI 1020 mild steel drilling is also considered. Finally, ANOVA is employed to investigate the impact of input parameters on the response of the current study.

3. Materials and Methods

3.1. Workpiece Material. This study used AISI 1020 mild steel with a small cylindrical workpiece measuring 130 mm in length, 40 mm in width, and 13 mm in thickness. The workpiece was mounted on a customized-built dynamometer, and the temperature was measured by connecting a thermal sensor to a computer, as illustrated in Figure 1. The workpiece was held in place by a specially developed and installed fixture in the dynamometer. The mechanical and thermal properties of AISI 1020 mild steel are shown in Table 2.

3.2. Cutting Tool, Cutting Parameters, and Machine Setup. HSS is used for dry conditions of mild steel [30]. The HSS has a point angle of 130° and a helix angle of 30°, as shown in Table 3. Drills often use a helix angle between 12° and 38° depending on the application; however, 30° is generally accepted as the standard [31]. A significant point angle and a large helix angle are also advantageous for decreasing burr development, enhancing chip removal, and reducing material sticking to the drill, which results in BUE [32].

Experimentations were carried out on a vertical milling machine for the drilling operation of AISI 1020 mild steel using cutting parameters, as shown in Table 3. The vertical milling machine has the maximal *f* and *n*of 12.4 mm/rev and 1010 rpm, respectively. Therefore, the combinations of drilling input parameters were selected based on previous literature, and their values were taken based on available milling machine specifications. It is an established observation that cutting tool vibration has a high ramification on drilling performance because higher vibration causes poor-quality holes with low accuracy [33]. The workpiece was positioned and secured on the machine table using nuts and bolts to reduce the vibrations. A force dynamometer comprised of sensors, actuators, and a transducer was used to measure the thrust force and torque induced on the workpiece, as shown in Figure 1(a). The torque and thrust force absorbed during the cutting process was measured with the help of a piezoelectric dynamometer, as shown in Figure 1(a), and data were recorded through a data acquisition device with a little 0.02% error in accuracy. The piezoelectric dynamometer comprises three-component sensors. Each sensor contains three quartz plates that transform forces into electric charges. Moreover, the charge amplifier converts the electric charges into voltage signals with the help of a high-isolated cable, while data processing is handled through Kistler's Dyno Ware software. The experimentation was done on a vertical milling machine (Model: Victoria-Elliott U2, London, UK). MATLAB was used to record data and display real-time graphs for the analysis. The equipment's details and experimental conditions are presented in Table 4.

3.3. Thermal Measurement. During drilling, temperature was measured using an infrared thermal sensor (Model: OS-180-USB-LSTL, Omega, United Kingdom). The thermal sensor was attached to the head of a vertical milling machine using a magnetic stand, as illustrated in Figure 1(b). A laser was positioned on a thermal sensor lens to precisely aim the infrared sensor at a drilled hole for accurate readings. After recording the data, the lens was carefully removed to expose the thermal sensor lens.

3.4. Postdrilling Experiments and Simulation. A simulation of the AISI 1020 mild steel has been carried out using Deform 3D software at various process conditions. The numerical model was first validated with the experimental data and the results are made on the following investigations. The numerical model was verified using experimental data through an in-depth contrast between simulation and actual experimentations in the drilling process. Comparing the simulation's predictions for axial load, torque, and temperature with the relevant experimental results was one of the validation's main requirements. The validation procedure increased confidence in the numerical model's ability to forecast and optimize mild steel machining parameters by confirming that it accurately represented the physical drilling conditions. Moreover, all the tests were performed under dry drilling conditions to reduce the cost and problems associated with chip recycling. It was also determined that it was measured using the Ra tester Mitutoyo (SJ-201). To ensure that the measurements were correct, the walls of each hole were cleaned using high-pressure air.

3.5. Analysis of Variance. Statistical techniques have become prevalent in various domains, such as engineering, agriculture, social science, and management. One such technique is the analysis of variance (ANOVA), which is used to determine the significance of data input factors on output responses [34]. Through ANOVA, researchers can perform hypothesis testing to identify the factors that influence the outcome of experiments. In the past, researchers commonly used a 95% confidence interval to evaluate ANOVA results. A confidence interval of 95% indicates a mere 5% probability of inaccurate estimation.

4. Result and Discussion

4.1. FE Modeling and Simulation. The present investigation involved the development of a finite element model using Deform 3D software. Flowchart for Deform simulation in the drilling process is shown in Figure 2.

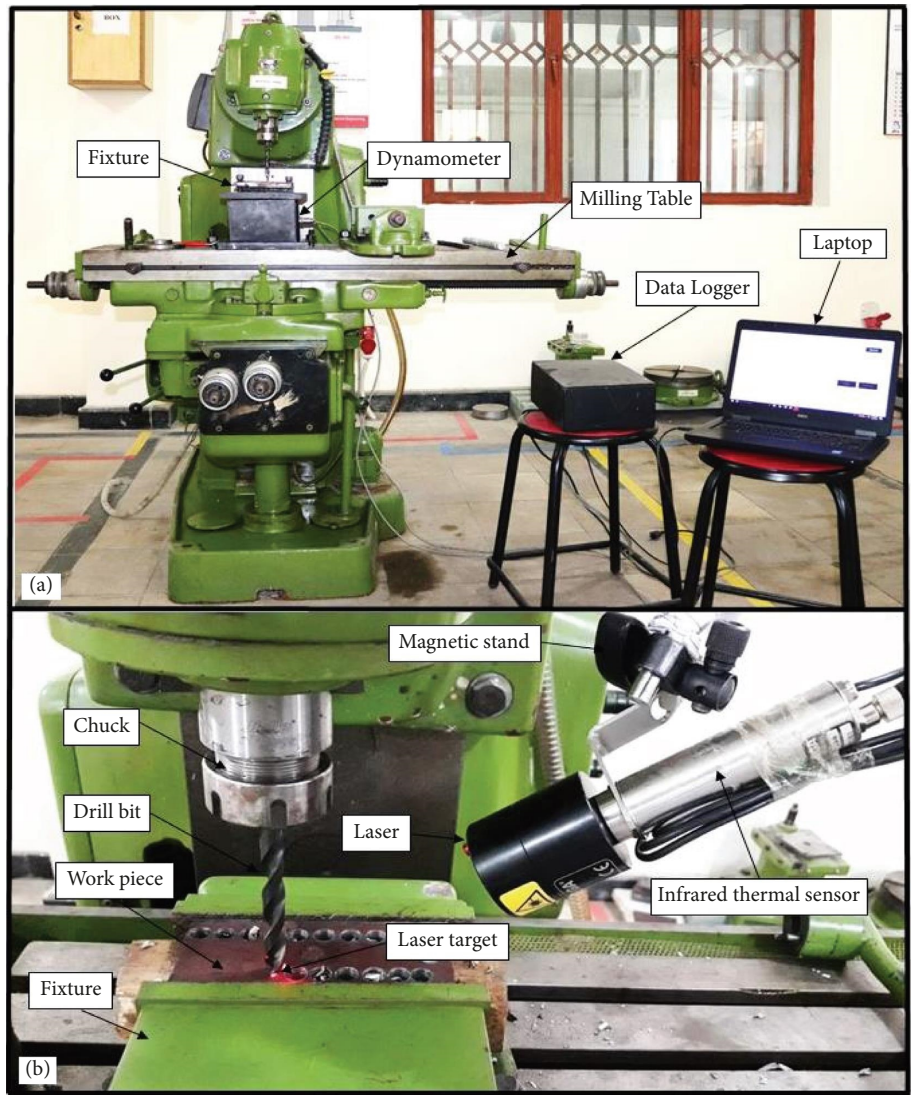

Figure 1: (a) Experimental setup for cutting force measurements. (b) Thermal measurement.

Table 2: Mechanical and thermal properties of workpiece material (AISI 1020 mild steel) [29].

Parameters	Values
Density	7.87 g/cm^3
Tensile strength	420 MPa
Yield strength	350 MPa
Modulus of elasticity	250 GPa
Poisson's ratio	0.29
Specific heat capacity	599 J/kg-K
Thermal conductivity	51.9 W/mK
Shear strength	235 MPa

Table 3: Cutting parameter.

Factors	Levels		
Spindle speed (rpm)	330	410	510
Feed rates (mm/rev)	0.12	0.20	0.30

Initiate the simulated drilling operation by first collating comprehensive data on the material properties, the geometry of the drilling tool, and various drilling parameters, such as feed rate and velocity, alongside the initial conditions. It is imperative to meticulously define the geometry of the drilling tool and the workpiece. For the latter, a finite element mesh must be constructed. This process involves decomposing the workpiece into smaller segments to facilitate a more manageable numerical analysis. In order to simulate the effects of clamping or holding fixtures, it is necessary to impose boundary conditions by securing the workpiece at predetermined locations. It is also crucial to accurately delineate the forces and constraints acting upon the drilling mechanism and assigning the material properties to the finite elements using the material chosen for the workpiece. Finally, specify the nature of the analysis, whether static, dynamic, thermal, or another type. Determine the temporal intervals and establish criteria for convergence within the simulation framework. Construct the comprehensive stiffness matrix by integrating the stiffness matrices of individual elements. Proceed to solve the system of equations to deduce the displacements and stress

Table 4: Equipment detail and experimental conditions.

Workpiece material	AISI 1020 mild steel having $L = 32$ mm and $D = 19$ mm
Drill bits	HSS drill bit having $D = 10$ mm, $\psi = 30^{\circ}$ and $\theta_{PA} = 130^{\circ}$, $L = 133$ mm and $L_{cutting} = 87$ mm
Machine tool	Vertical milling machine
Drilling condition	Dry conditions
Thermal sensor	Infrared type, min/max temp measurement $(450^{\circ} - 842^{\circ})/(2000^{\circ} - 3632^{\circ})$

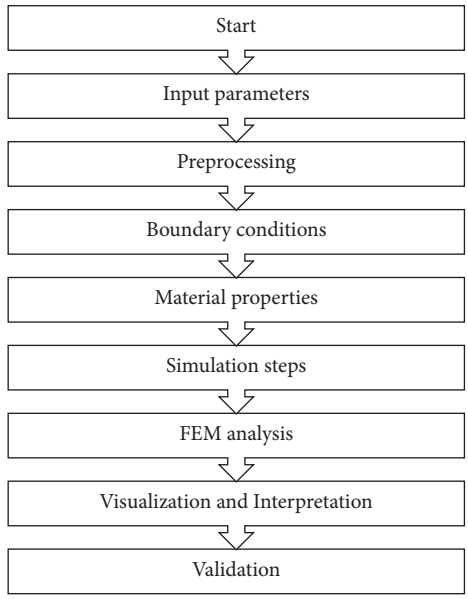

Figure 2: Deform simulation and FEM steps.

states within the workpiece. Conduct a thorough analysis of the outcomes to gain insights into deformation patterns, stress distributions, and other pertinent phenomena. Employ suitable software tools for the visualization of these results. Interpret the findings from the simulation to comprehend the workpiece's behavior under drilling conditions. Compare and contrast the simulation outcomes with empirical data or established benchmarks to validate the results. Identify potential areas for enhancement or optimization within the drilling process.

The FE model requires the input of temperature and mechanical and geometrical data to represent the tool and workpiece. The mesh density was increased in areas with large plastic strain gradients to achieve accurate results and enhance the solution convergence, thereby minimizing the interpolation error. The workpiece was fixed in all three perpendiculars, while the drill bit was allowed to move in the y-direction (f) and rotate about the y-axis with n chosen for the current study during the FE simulation.

In the Finite Element Analysis (FEA) simulation, the workpiece employed is manufactured from AISI 1020 mild steel, whereas the cutting tool is made using HSS. In this process, the chips are separated utilizing remeshing techniques based on the strain alteration criteria. The workpiece is treated as a deformable object, and the elements near the cutting lip of the drill bit are inclined to undergo significant distortion due to the plastic deformation of chips. Consequently, the Jacobean matrix yields a negative value. Therefore, remeshing techniques are vital to substitute the distorted elements with more appropriate shapes. Upon remeshing, the present deformation, strain, stresses, and various parameters are transmitted to the new mesh, and the analysis is carried forward. The shear strength of a material is often associated with multiple constitutive material laws that account for temperatures, strain rates, and strains [35]. However, this research employed a piecewise-rectangular-shaped material model to consider diverse temperatures, strain rates, and strains in the drilling process of AISI 1020 mild steel. The study depicts temperature contours, strain impacts, and damage in Figures 3 and 4, respectively. To have an in-depth knowledge of AISI 1020 mild steel mechanical and thermal behaviors during the machining process, it is imperative to consider temperature contours, strain impacts, and damage in the mild steel drilling simulation [36]. The distribution of heat produced during drilling can be shown using temperature contours. High temperatures can impact tool wear, cause thermal strains, and change a material's characteristics. Temperature contour monitoring is crucial to avoid excessive heat that could cause material degradation, hardness changes, or even thermal cracking [37].

Figure 3 shows the maximum temperature is distributed at the center of the hole with 319°C whiles the minimum temperature of blue color at the outer region of the workpiece. Information regarding the material's deformation and structural changes during drilling can be obtained by analyzing strain impacts. The overall integrity of the drilled hole may be compromised by plastic deformation caused by excessive strain, which also changes the material's mechanical characteristics. Understanding strain distribution depends on predicting material behavior, identifying potential failure zones, and maximizing drilling settings to reduce negative impacts [38].

Figure 4(a) shows the maximum strain effective at the center of the workpiece, showing the maximum force inserted in the center of the hole. Evaluating damage, such as material removal or microstructural alterations, helps determine how the mild steel drilling process will affect it. Damage analysis highlights possible structural problems in the workpiece, tool wear, and chip formation [39]. To ensure the long-term durability of the tool and the machined product, it is crucial to identify the areas of damage and optimize tool geometries and cutting rates. Moreover,

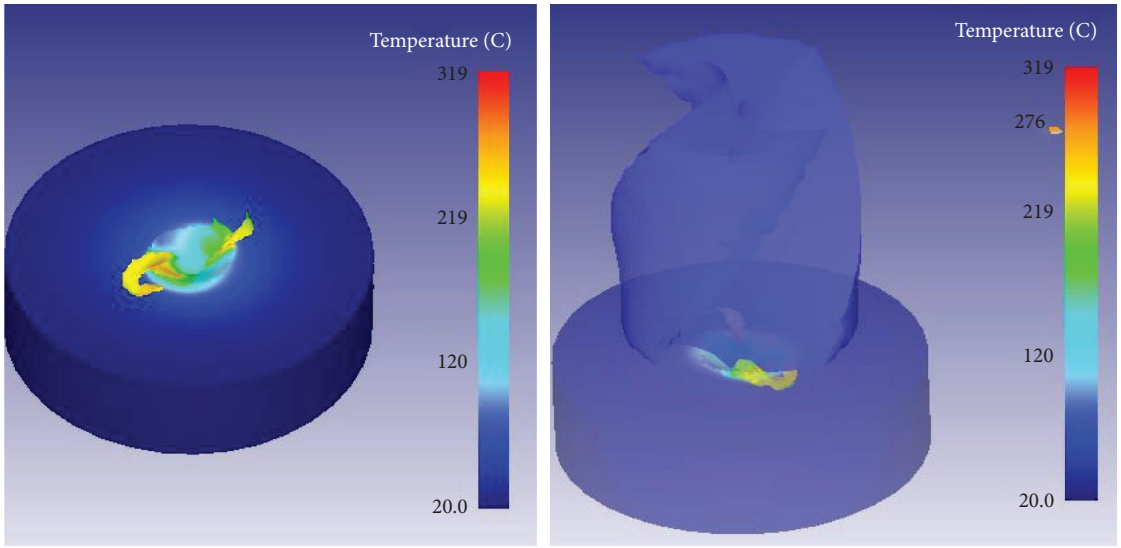

Figure 3: Temperature contours.

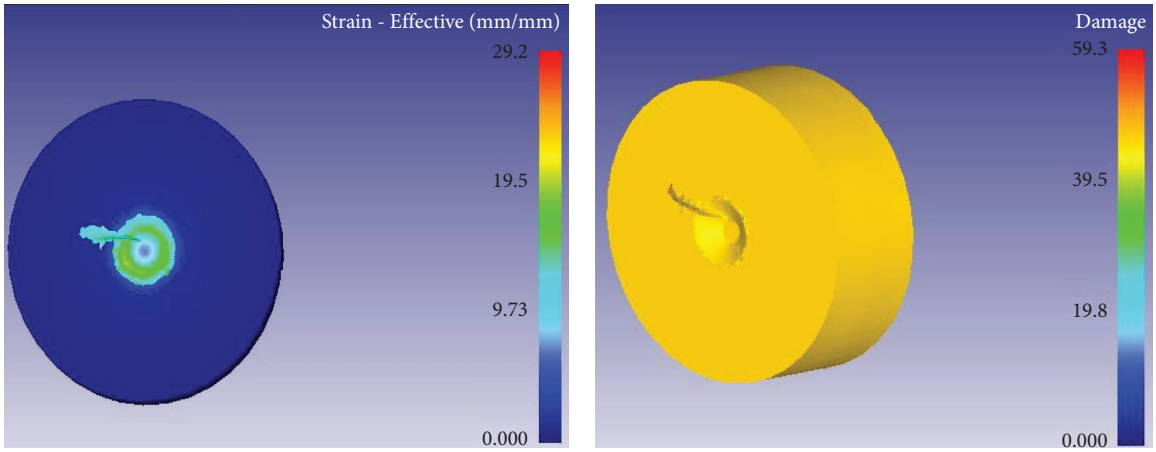

(a) (b)

Figure 4: (a) Strain effective, (b) Damage.

Figure 4(b) shows the damage analysis of the workpiece, showing maximum damage in the center of the hole. Furthermore, Figure 5 portrays the chip formation after successfully implementing the meshing technique. Moreover, Figure 5 also shows small and discontinuous chips as they are preferable over long and continuous ones, as the latter tend to tangle around the drilling tool, resulting in decreased productivity [40].

4.2. Analysis of Cutting Forces. The cutting forces heavily influence the drilling process, as they play a significant role in determining the quality of holes, cutting tool lifespan, power consumption, and vibration [41]. In machining, the cutting forces are required to shear the material, and they reflect the overall toughness of the material during the operation [42]. Drilling operations, in particular, are affected by two types of cutting force: the axial force (thrust force) and torque. The thrust force (Fz) acts perpendicularly to the workpiece surface, while torque (Mz) represents the force the machine spindle requires to rotate the cutting tool. However, the contribution of forces generated in the x and y directions is insignificant in drilling as compared to Fz and Mz [43]. High thrust force can lead to a shorter lifespan of the cutting tool and early failure, whereas high torque indicates a larger amount of friction between the workpiece and the tool, resulting in more heat generation and high temperature in the region where the tool contacts the workpiece [44]. However, low torque and thrust force can be achieved at a f and high n [45]. Although other forces created in the x and y directions are present in drilling, they are insignificant compared to Mz and Fz and are thus ignored in the current study [43]. Moreover, cutting forces significantly impact hole quality, surface quality, power consumption, vibration, and cutting tool lifespan, all of which are critical aspects of the drilling process [41].

4.2.1. Thrust Force. In drilling operations, the thrust force (Fz) holds significant importance as it determines the hole quality and the tool's wear [46, 47]. As depicted in Figure 6,

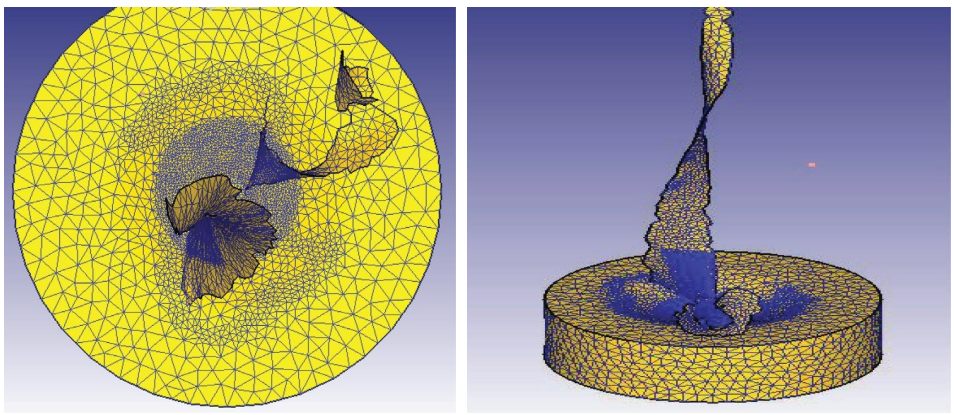

Figure 5: Drilling operation and chip formation.

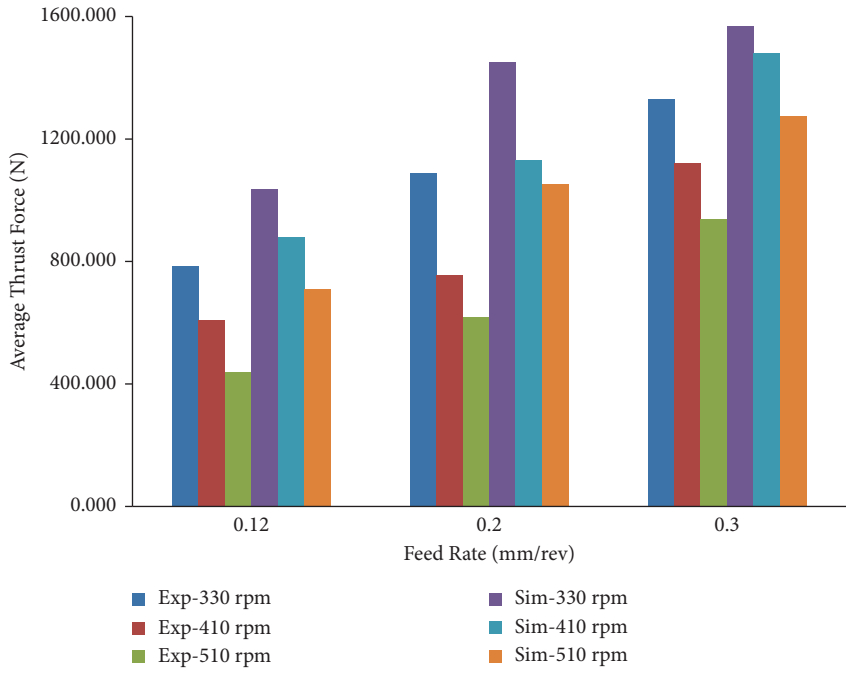

Figure 6: Average thrust force validation.

Fz has been studied through experimental and numerical methods, and the results obtained from both methods are in good agreement. The comparison between the numerical and experimental values shows 91.53% agreement. The relationship between thrust force variation and f and n parameters has also been investigated. The study suggests that Fz is directly proportional to f and inversely proportional to n.

According to the findings presented in Figure 6, the maximum Fz obtained from simulation tests was recorded at 1570 N, which is greater than the maximum experimental value of 1430 N. The observed 9.79% error in the experimental results is attributed due to limitations in the precision of sensors, environmental factors, and machine dynamics during experimentations. The results further indicate that a rise in f led to a corresponding increase in the Fz value during both simulation and experimentation, while the rise in n dropped the Fz value. The maximum and minimum Fz values for both simulation and experimental results were recorded at f values of 0.3 and 0.12 mm/rev and n values of 330 and 510 rpm, respectively. Notably, a significant decrease in the Fz was observed with increased n from 330 rpm to 510 rpm.

The average Fz achieved during experimentation is depicted in Figure 7. The graph shows a perceptible drop in Fz with a rise in n from 330 to 510 rpm. This reduction can be attributed to the heat generated in the penetration area of the drilled hole, which lowers the material's hardness and, hence, results in a lower Fz [48]. Additionally, the Fz decreases due to increased material ductility caused by n drilling temperature [49, 50]. Figure 7 demonstrates that a rise in f from 0.12 to 0.3 mm/rev leads to rise in Fz. This phenomenon can be attributed to the rise in penetration load in the workpiece with an increase in chip thickness [51, 52].

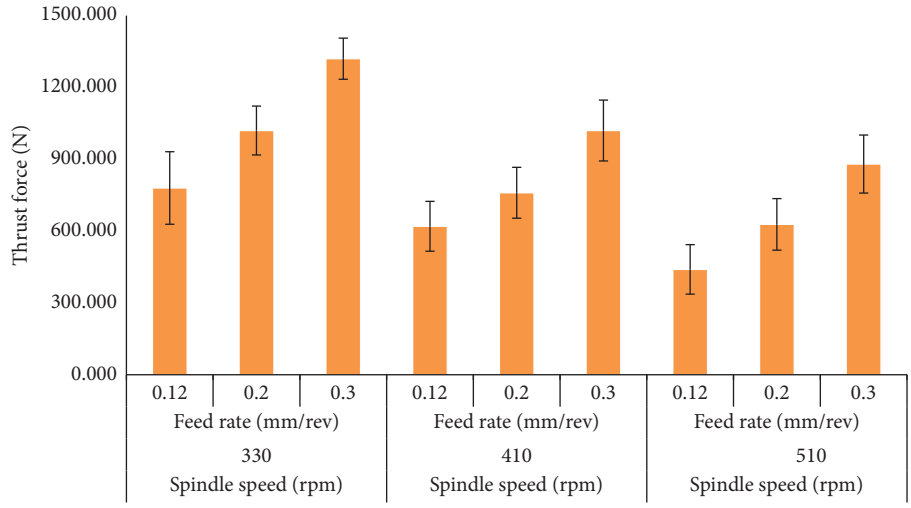

Figure 7: Thrust force variations with respect to *f* and *n*.

The material hardness also contributes to the Fz, as a high hardness level can cause greater wear to the tool and generate more Fz [50]. *P* values are frequently used in ANOVA tables to indicate the statistical significance levels. The observed variations in the response variable (thrust force and torque) are statistically significant if the *P* value is less than the selected significance level, typically 0.05. Table 5 reveals that both *f* and *n* significantly influence axial load or thrust force. However, *f* has a more significant impact on Fz than *n*.

The ANOVA results indicated that *f* contributes the most to thrust force, with a percentage contribution of 61.73% followed by *n*, with a percentage contribution of 37.09%. A low *P* value for Table 5 suggests that the parameters (*f* and *n*) significantly affect Fz, which is likely to represent the factors controlling thrust force. If substantial, it suggests that Fz during drilling is significantly impacted by *n* and *f* variations.

4.2.2. Torque. The torque variation in both simulation and experimental results is seen in Figure 8. The achieved results are approximately 90% in agreement with the experimental results. The model's ability to predict machining results is demonstrated by successfully integrating simulation and experimental results, with an approximate torque agreement of 90%. This high degree of agreement may result from appropriate simulation parameter calibration using experimental data, which ensures the model accurately depicts the complexities of the machining process. Variations, however, could occur because of intrinsic complexity that needs to be fully considered because of sensor accuracy limitations, environmental influences, and machine dynamics during experiments. Even with the simulation's useful prediction tool, certain complex and dynamic aspects of machining processes might still be difficult to represent accurately. The variation in torque depends upon both *f* and *n*. Torque is directly related to the *f* and inversely related to *n*. The torque increases from 0.12 to 0.3 mm/rev and decreases with increasing *n* from 330 to 510 rpm. The maximum simulation value of torque at 0.3 *f* reaches 6.777 N-m, while in experimentation, the maximum torque obtained at 0.3 *f* is 6.490 N-m with an error difference of 4.42%. The behavior of torque in both simulation and experimentations with increasing *f* is also presented in Figure 8. Results indicate that torque rises with the increase in *f*. However, torque decreases with increased *n* from 310 to 510 rpm.

According to the findings presented in Figure 9, a rise in *n* from 330 rpm to 510 rpm results in a decrease in the torque value from an average of 6.50 N-m to 3.40 N-m. Additionally, as highlighted in Figure 9, high *n* leads to a heightened generation of temperature between the tooltip and the cutting zone. The resultant increase in temperature causes the material in the vicinity of the drilled hole to liquefy, thereby resulting in the production of a softer material that enables the shearing layers to slip easily with relatively low force compared to low temperature and hard material [53]. This phenomenon translates to high *n* and low torque.

Figure 9 illustrates the torque behavior with respect to increasing *f*. The findings reveal that torque rises proportionally with the rise in *f*. This can be attributed to the fact that a larger *f* leads to faster penetration of the drill bit, resulting in larger chip thickness and MRR, thereby causing an increase in torque [54]. Moreover, it has been observed that the tooltip necessitates maximum force to remove the material with maximum chip thickness [55]. This force accounts for the high values of torque produced. Furthermore, the ANOVA results presented in Table 6 demonstrate that *f* has a more significant impact on torque than *n*. Moreover, Table 6 indicates that *f* contributes the most to torque, with a percentage contribution of 59.87%, respectively, followed by *n*, with a percentage contribution of 38.89%.

4.3. Temperature. In the process of drilling, the rise in temperature is contingent upon the machining parameters, namely, *f* and *n* [56]. The finite element model of the drilling temperature is validated with experimental results, as shown in Figure 10. A maximum error of 8.10% was reported, indicating high thermal coherence between simulated and

Table 5: ANOVA results for thrust force.

Source	DF	Seq SS	Adj SS	Adj MS	*F* value	*P* value	Contribution (%)
Model	4	652911	652911	326455	168.25	0.001	98.82
Linear	4	652911	652911	326455	168.25	0.001	98.82
Spindle speed	2	245072	245072	122536	63.15	0.001	37.09
Feed rate	2	407839	407839	203919	105.10	0.001	61.73
Error	4	7761	7761	1940			1.17
Total	16	660672					100.00

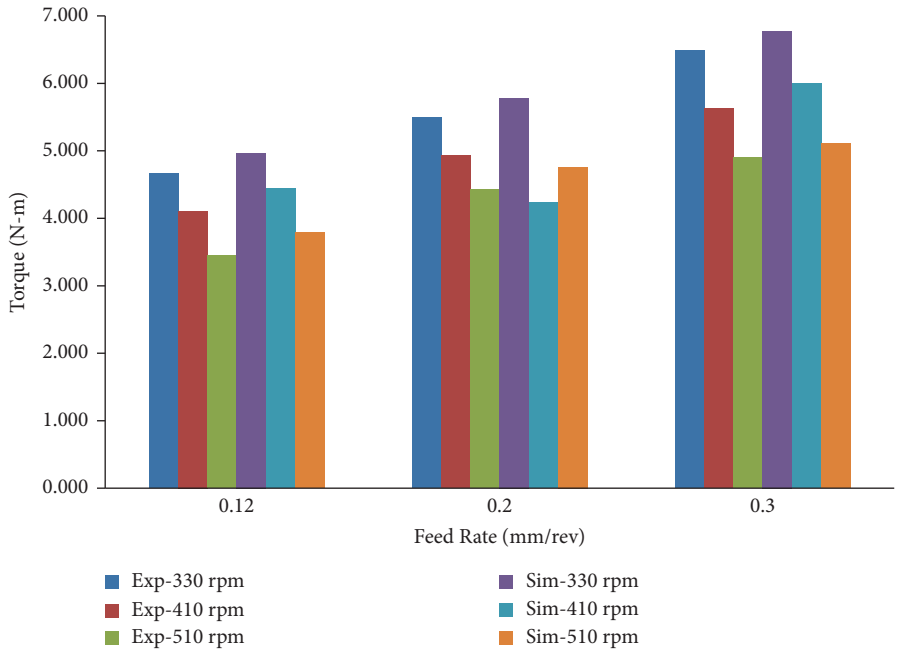

Figure 8: Average torque validation.

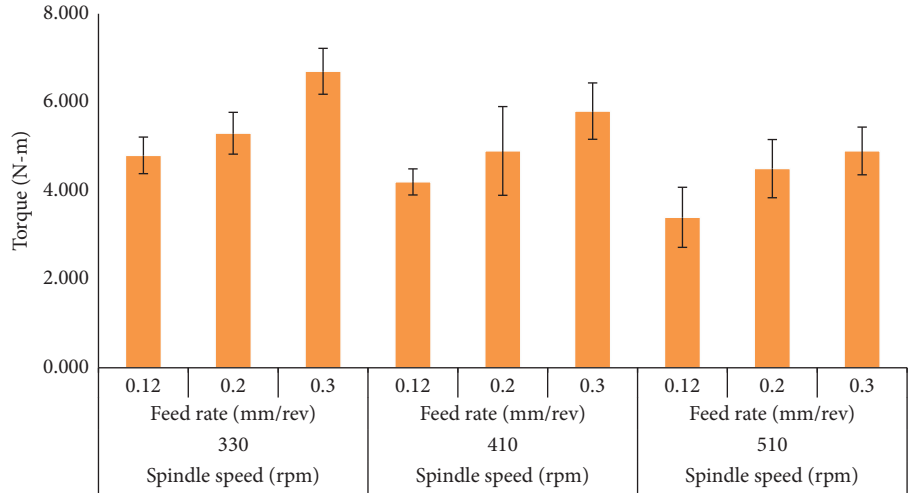

Figure 9: Torque variations with respect to *f* and *n*.

experimental temperatures. *n* has a substantial impact on temperature and significantly influences the tool's performance, especially at higher speeds [57]. High *n* may generate frictional heat at the interface between the tool and the workpiece. In the current study, temperature is directly related to *n* and *f*. The temperature increases with increased *n* from 330 mm/rev to 510 mm/rev.

As shown in Figure 11, an increase in *n* leads to a noticeable upsurge in temperature. This rise in temperature causes intense friction between the workpiece and the

Table 6: ANOVA results for torque.

Source	DF	Seq SS	Adj SS	Adj MS	*F* value	*P* value	Contribution (%)
Model	4	6.33298	6.33298	3.16646	160.19	0.001	98.76
Linear	4	6.33298	6.33298	3.16646	160.19	0.001	98.76
Spindle speed	2	2.49391	2.49391	1.24693	63.08	0.002	38.89
Feed rate	2	3.83907	3.83907	1.91953	97.11	0.001	59.87
Error	4	0.07907	0.07907	0.01977			1.23
Total	16	6.41205					100.00

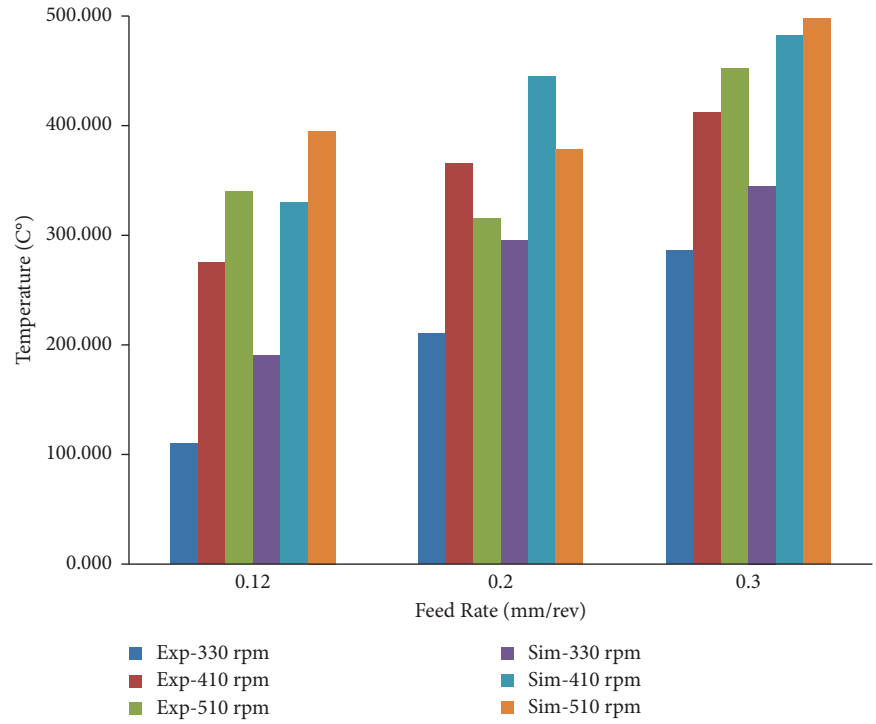

Figure 10: Average temperature validation.

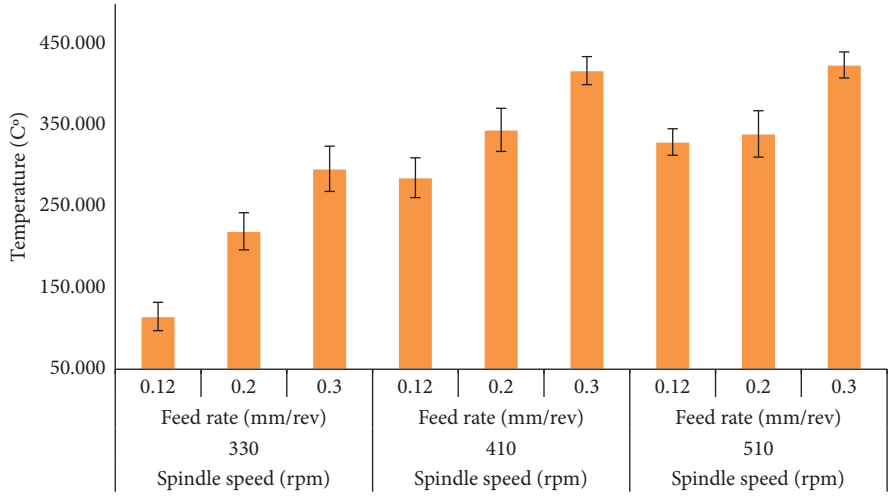

Figure 11: Temperature variations with respect to *f* and *n*.

rotating tool [58]. According to Nouari et al. [32], a decrease in tool life leads to a decrease in temperature. Moreover, they reported that *f* and *n* contribute to the temperature rise. Higher *n* causes plastic deformation, leading to temperature escalation. In contrast, when *f* is high, it results in a longer contact length between the chips and the tool, which

increases in temperature. According to Bates [59], rise in *f* results in a rise in the area of primary and secondary shear planes, which facilitate the dissipation of more heat in the tool and workpiece. Additionally, high *f* and the generation of continuous chip formation lead to an increase in tooltip temperature [60]. Figure 11 depicts the trend of increasing temperature with an increase in *f*. Heightening the tool's depth of travel increases the MRR and results in high temperatures [61]. The variation observed at the start of the graphs is due to the fact that the temperature of the workpiece and tool was not set to room temperature for the subsequent experiment. Based on the ANOVA results presented in Table 7, *n* has a greater impact on temperature compared to *f*.

4.4. Surface Roughness. Surface roughness Ra is a prevalent industry metric employed to gauge the roughness of surfaces [62, 63]. In holes, this metric can assume higher values, leading to elevated material fatigue and wear, adversely impacting the production process and increasing manufacturing expenses. Machining parameters, such as the vibration induced on the workpiece and the cutting tool's geometry, can significantly influence *Ra* [64].

According to Figure 12, the average Ra with respect to *f* and *n* is significantly influenced by both factors. The graph demonstrates a gradual decrease in Ra values as *n* increases. The minimum and maximum Ra values are observed at 510 rpm and 330 rpm, respectively. However, an increase in *f* from 0.12 mm/rev to 0.3 mm/rev leads to an increase in Ra. The lowest Ra value of 4.22 μm and the highest Ra value of 5.88 um are observed at *f* values of 0.12 mm/rev and 0.3 mm/rev, respectively. According to Olabi and Hashmi [65], there is a decrease in Ra with an increase in *n* due to two reasons. Firstly, the contact between the chip and the tooltip is shorter, reducing the Ra of the hole's internal surface. Secondly, the surface temperature of the hole wall, which softens the material, decreases the resistance against the tooltip [66]. Additionally, increased material ductility due to increased temperature might contribute to this phenomenon [67].

The Ra value is observed to increase with an increase in *f* for several reasons. Firstly, as the process frequency increases, the workpiece materials are prone to laceration due to the high temperature [68]. Secondly, the Ra value increases with increased *f* due to chatter phenomena and drilling vibrations [68]. Thirdly, increased *f* leads to a higher material removal rate, resulting in poor hole quality [68]. Additionally, the chip volume increases with an increase in *f*, as the thick chip formation produces a low shear angle and a high thrust force [69, 70]. The deformation of this thick chip layer requires a high thrust force, which induces more aggressive vibration in the tool and ultimately leads to a poor surface finish [2, 71]. Furthermore, from Table 8, it can be concluded that *f* has a more significant impact on Ra than *n*.

4.5. Chip Formation. Chip morphology has a major effect on the drilling process because it affects material removal efficiency, heat dissipation, and tool wear. Well-defined chips help evacuate heat effectively, minimizing thermal damage to the tool and workpiece [72]. In machining, the chip generation process directly impacts the integrity of the machined hole, surface finish, and dimensional accuracy. A proper chip formation is essential in order to minimize tool wear, reduce heat production, and limit chip recutting—all of which lead to improved hole quality. Achieving targeted machining results and improving the general quality of drilled or machined holes depend heavily on understanding and optimizing chip formation mechanisms [73].

Metal cutting chips can be categorized into four main types based on their geometrical properties: continuous, discontinuous, segmented, and lamellar. Drilling becomes more efficient when continuous chips are used since they tend to increase surface finish and decrease tool wear. In addition to increasing tool wear, discontinuous chips can degrade surface finish. Based on the particular needs of the machining process, segmented and lamellar chips can achieve a balance by slightly affecting tool wear and preserving a satisfactory surface finish, affecting overall drilling efficiency [72]. The formation of a continuous chip is facilitated by using a ductile material and a tool with sharp edges with high *n* values and low *f* values [74]. On the other hand, when machining hard materials, it is preferred to form discontinuous chips as they result in a smooth surface finish. Discontinuous chips are formed by machining ductile materials with small rake angles and low *f* values, while continuous chips tend to stick to the tool and produce a Built-Up Edge (BUE). Furthermore, machining hard or brittle materials results in the formation of discontinuous chips [75].

In the machining industry, segmented and lamellar chips are two types generated during drilling. Segmented, discontinuous chips are produced at low *f* and *n*, while lamellar chips, which are semicontinuous, are generated at high *n* and *f* [74]. It is widely accepted that uniformly small segmented chips are preferred during drilling. The chips' size and fragmentation significantly impact the prevention of the drilling tool from breaking and the smoothness of the process [76, 77]. During the machining of mild steel, small and discontinuous chips are desirable because long and continuous chips easily get tangled around the drilling tool, due to which productivity of the manufacturing process decreased. In the case of machining mild steel, small and discontinuous chips are preferable over long and continuous ones, as the latter tend to tangle around the drilling tool, resulting in decreased productivity [40].

The results of a study on the drilling of AISI 1020 mild steel are presented in Figure 13. The findings indicate that the chips' length increases while their thickness decreases with an increase in *n*. This phenomenon is attributed to the material ductility resulting from extreme temperatures experienced at high *n* values, ultimately producing longer chips [78]. Conversely, a decrease in the length and an increase in the thickness of the chips produced lead to the formation of short and segmented chips. This occurs due to the high thrust force generated by the high chip thickness, which makes the chip more susceptible to breaking as the sectional area of the chip increases and stiffness is absorbed

Table 7: ANOVA results for temperature.

Source	DF	Seq SS	Adj SS	Adj MS	*F* value	*P* value	Contribution (%)
Model	4	98293	98293	49146.3	173.45	0.001	98.86
Linear	4	98293	98293	49146.3	173.45	0.001	98.86
Spindle speed	2	67362	67362	33681.0	118.87	0.001	67.75
Feed rate	2	30931	30931	15465.3	54.58	0.002	31.11
Error	4	1133	1133	283.3			1.14
Total	16	99426					100.00

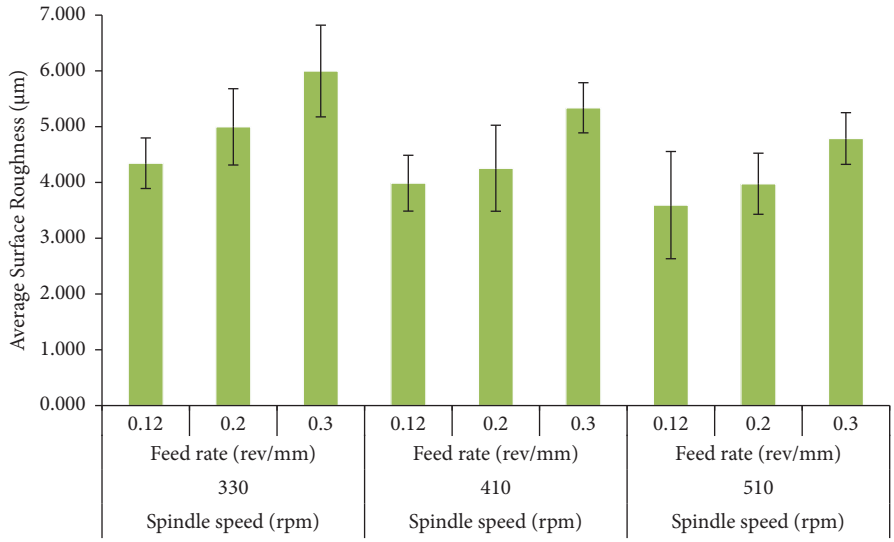

Figure 12: Average surface roughness.

Table 8: ANOVA results for surface roughness.

Source	DF	Seq SS	Adj SS	Adj MS	*F* value	*P* value	Contribution (%)
Model	4	4.57666	4.57666	2.28833	121.72	0.003	98.38
Linear	4	4.57666	4.57666	2.28833	121.72	0.003	98.38
Spindle speed	2	1.49708	1.49708	0.74854	39.82	0.002	32.18
Feed rate	2	3.07958	3.07958	1.53979	81.90	0.001	66.20
Error	4	0.07520	0.07520	0.01880			1.62
Total	8	4.65186					100.00

[76, 79]. While both *f* and *n* have a significant impact on chip formation, it is observed that *n* has a more significant influence than *f* during the chip formation process of AISI 1020 mild steel.

The research findings on the AISI 1020 mild steel drilling process have essential applications for actual manufacturing facilities. Manufacturers may strategically optimize their machining operations to improve efficiency and product quality by determining the correlations between *n*, *f*, and other process parameters, including thrust force, torque, temperature, and surface roughness. From a practical standpoint, these established correlations provide helpful information for determining the optimal combinations of *n* and *f* to attain desired results. For example, manufacturers can choose the best cutting conditions that reduce tool wear and energy consumption by using the relationship between *n*, Fz, and Mz. The study results can be used to determine a balance between *n* and *f* that efficiently regulates temperature levels. Temperature control during drilling is essential for preventing overheating. Additionally, the relationship with Ra gives manufacturers a valuable tool to adjust their machining parameters to suit specific criteria for surface finish, ensuring the creation of high-quality components. The findings can also aid in developing data-driven automation and process optimization strategies in manufacturing environments. Manufacturers can apply existing relationships to computer numerical control (CNC) systems or machining algorithms, enabling real-time *n* and *f* modifications based on specific material properties and machining conditions. With this flexibility, the drilling process for AISI 1020 mild steel is more precise and efficient, per the emerging trend of smart manufacturing and Industry 4.0 initiatives. The study's practical implications go beyond the lab; it offers manufacturers helpful information that they

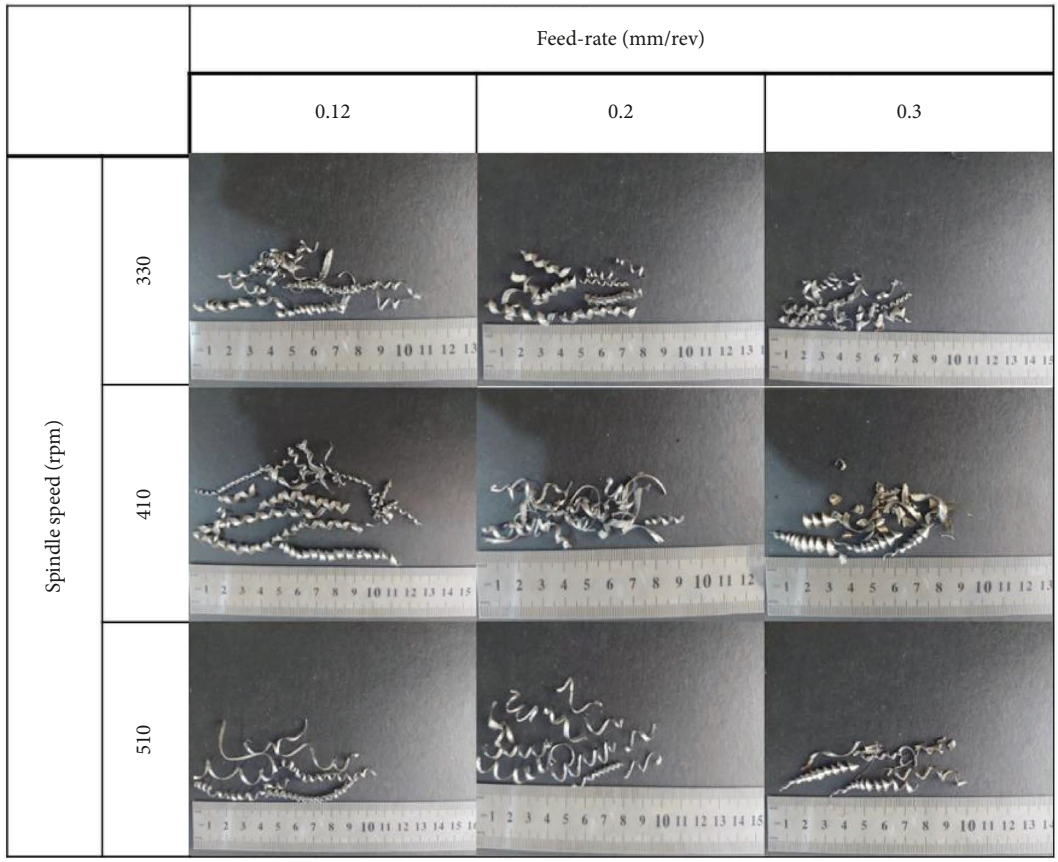

Figure 13: Chip formations on different spindle speed and feed rate.

can utilize to improve their machining procedures, reduce costs, and consistently produce high-quality components for use in real-world applications.

5. Conclusions

The present investigation involved conducting a Deform simulation and experimental study on AISI 1020 mild steel. The study examined the impact of varying *n* and *f* on process parameters such as Fz, Mz, *t*, Ra, and chip formation. The key outcomes of the study are outlined as follows.

The comparison between the simulation and experimental values, with a 2%–10% error in the experimental study, indicates that the thrust force increases with a rise in feed rate, while its value decreases when the spindle speed increases. Based on the ANOVA results, it can be inferred that the feed rate has a greater influence on thrust force than spindle speed, as it has a percentage contribution of 61.73%, while spindle speed has a percentage contribution of 37.09%.

The relationship between torque, spindle speed, and feed rate is of great importance in machining processes. Numerical and experimental values reveal that torque values exhibit an inverse correlation with spindle speed and a direct correlation with feed rate. Moreover, statistical analysis conducted by ANOVA indicates that the feed rate has a more significant impact on torque than spindle speed. Additionally, the contribution of feed rate to torque (59.87%) was higher than that of spindle speed of 38.89%.

Experimental results show that both spindle speed and feed rate significantly impact temperature, with higher values for both parameters leading to increased temperatures. Specifically, an increase in spindle speed and feed rate causes a rise in temperature. However, statistical analysis using ANOVA revealed that spindle speed had a greater influence on temperature than the feed rate, contributing 67.75% to the feed rates of 31.11%.

The study reveals that the surface roughness of a material is directly proportional to the feed rate and inversely proportional to the spindle speed. Furthermore, the ANOVA analysis indicates that the feed rate had a greater influence on the surface roughness than the spindle speed. The feed rate had a percentage contribution of 66.20%, whereas the spindle speed contributed 32.18%.

The shape of the chip is significantly influenced by spindle speed and feed rate. An increase in spindle speed from 330 to 510 rpm produces a long continuous chip. Conversely, an increase in feed rate from 0.12 mm/rev to 0.3 mm/rev forms a thick, short, and discontinuous chip.

Data Availability

Data will be made available by the corresponding author upon reasonable request.

Conflicts of Interest

The authors declare that there are no conflicts of interest.

References

[1] C. S. J. Mario, A. Machado, W. F. Sales, E. O. Ezugwu, and M. Barrozo, *Machining of aluminum alloys: A Review*, vol. 86, no. 9, pp. 3067–3080, 2016.

[2] M. Kurt, E. Bagci, and Y. Kaynak, "Application of Taguchi methods in the optimization of cutting parameters for surface finish and hole diameter accuracy in dry drilling processes," *The International Journal of Advanced Manufacturing Technology*, vol. 40, no. 5-6, pp. 458–469, 2009.

[3] N. Habib, A. Sharif, A. Hussain et al., "Analysis of hole quality and chips Formation in the dry drilling process of Al7075-T6," *Metals*, vol. 11, no. 6, p. 891, 2021.

[4] A. Akhavan Farid, S. Sharif, and M. Idris, "Chip morphology study in high speed drilling of Al–Si alloy," *The International Journal of Advanced Manufacturing Technology*, vol. 57, no. 5-8, pp. 555–564, 2011.

[5] M. Aamir, M. Tolouei-Rad, K. Giasin, and A. Nosrati, "Recent advances in drilling of carbon fiber–reinforced polymers for aerospace applications: a review," *The International Journal of Advanced Manufacturing Technology*, vol. 105, no. 5-6, pp. 2289–2308, 2019.

[6] M. Aamir, A. Sharif, M. Z. Zahir, K. Giasin, and M. Tolouei-Rad, "Experimental assessment of hole quality and tool condition in the machining of an aerospace alloy," *Machines*, vol. 11, no. 7, p. 726, 2023.

[7] K. Giasin, A. Hodzic, V. Phadnis, and S. Ayvar-Soberanis, "Assessment of cutting forces and hole quality in drilling Al2024 aluminium alloy: experimental and finite element study," *The International Journal of Advanced Manufacturing Technology*, vol. 87, no. 5-8, pp. 2041–2061, 2016.

[8] P. K. Saraswati, S. Sahoo, S. P. Parida, and P. C. Jena, "Fabrication, characterization and drilling operation of natural fiber reinforced hybrid composite with filler (fly-ash/graphene)," *International Journal of Innovative Technology and Exploring Engineering*, vol. 8, no. 10, pp. 1653–1659, 2019.

[9] S. Aamer, A. Hussain, N. Habib et al., "Experimental investigation of hole quality and chip analysis during the dry drilling process of Al6061-T6," *Journal of Materials and Manufacturing*, vol. 2, no. 1, pp. 21–30, 2023.

[10] A. Sharif, "Study on burr formation, tool wear and surface quality in machining Al6063," *Journal of Materials and Manufacturing*, vol. 1, no. 2, pp. 1–9, 2022.

[11] M. T. Tamura, "An assessment of the drilling process employed by the hole-drilling method for residual stress measurements," 2016.

[12] A. Shash, M. K. El-Fawkhry, S. A. Abd El Rahman, I. S. Elmahallawi, and T. Mattar, "Improvement of mechanical properties and structure modifications of low carbon steel by inoculations with nano-size silicon nitride," *Journal of Nano Research*, vol. 47, pp. 24–32, 2017.

[13] N. Habib, A. Sharif, A. Hussain, M. Aamir, K. Giasin, and D. Y. Pimenov, "Assessment of hole quality, thermal analysis, and chip formation during dry drilling process of gray cast iron ASTM A48," *Engineer*, vol. 3, no. 3, pp. 301–310, 2022.

[14] A. Hussain, A. Sharif, N. Habib et al., "Effect of drilling process parameters on brass alloy 272 through experimental techniques," *Journal of Mechanical Engineering Research and Developments*, vol. 44.

[15] E. Ezugwu and Z. Wang, "Titanium alloys and their machinability—a review," *Journal of Materials Processing Technology*, vol. 68, no. 3, pp. 262–274, 1997.

[16] D. E. B. A. B. R. A. T. A. Dhupal, D. Panigrahi, S. Rout et al., "Generation of effusion holes on ultra-high temperature alloy by micro electro-discharge machining process," *Surface Review and Letters*, vol. 31, no. 02, 2024.

[17] M. Günay, İ. Korkut, E. Aslan, and U. Şeker, "Experimental investigation of the effect of cutting tool rake angle on main cutting force," *Journal of Materials Processing Technology*, vol. 166, no. 1, pp. 44–49, 2005.

[18] J. Nomani, A. Pramanik, T. Hilditch, and G. Littlefair, "Machinability study of first generation duplex (2205), second generation duplex (2507) and austenite stainless steel during drilling process," *Wear*, vol. 304, no. 1-2, pp. 20–28, 2013.

[19] A. N. Siddiquee, Z. A. Khan, P. Goel, M. Kumar, G. Agarwal, and N. Z. Khan, "Optimization of deep drilling process parameters of AISI 321 steel using Taguchi method," *Procedia Materials Science*, vol. 6, pp. 1217–1225, 2014.

[20] J. Cyril, A. Paravasu, J. Jerald, K. Sumit, and G. Kanagaraj, "Experimental investigation on performance of additive mixed dielectric during micro-electric discharge drilling on 316L stainless steel," *Materials and Manufacturing Processes*, vol. 32, no. 6, pp. 638–644, 2017.

[21] R. T. Bhole and R. Shelke, "Optimization of drilling process parameters for AISI 316L by using taguchi method," *International Journal of Scientific Research in Science, Engineering and Technology*, vol. 2, pp. 2395–1990, 2016.

[22] D. Sonowal, D. Sarma, P. B. Barua, and T. Nath, "Taguchi optimization of cutting parameters in turning AISI 1020 MS with M2 HSS Tool," *IOP Conference Series: Materials Science and Engineering*, vol. 225, p. 012186, 2017.

[23] T. Kıvak, G. Samtaş, and A. J. M. Cicek, "Taguchi method based optimisation of drilling parameters in drilling of AISI 316 steel with PVD monolayer and multilayer coated HSS drills," *Measurement*, vol. 45, no. 6, pp. 1547–1557, 2012.

[24] B. Shivapragash, K. Chandrasekaran, C. Parthasarathy, and M. Samuel, "Multiple response optimizations in drilling using Taguchi and grey relational analysis," *International Journal of Industrial Engineering Computations*, vol. 3, no. 2, pp. 765–768, 2013.

[25] S. Mahapatra, A. Das, P. C. Jena, and S. R. Das, "Turning of hardened AISI H13 steel with recently developed S3P-AlTiSiN coated carbide tool using MWCNT mixed nanofluid under minimum quantity lubrication," *Proceedings of the Institution of Mechanical Engineers-Part C: Journal of Mechanical Engineering Science*, vol. 237, no. 4, pp. 843–864, 2023.

[26] S. Pradhan, S. R. Das, P. C. Jena, and D. Dhupal, "Investigations on surface integrity in hard turning of functionally graded specimen under nano fluid assisted minimum quantity lubrication," *Advances in Materials and Processing Technologies*, vol. 8, no. sup3, pp. 1714–1729, 2022.

[27] J. Jena, A. Panda, A. K. Behera, P. C. Jena, S. R. Das, and D. Dhupal, "Modeling and optimization of surface roughness in hard turning of AISI 4340 steel with coated ceramic tool," *Innovation in Materials Science and Engineering*, vol. 2, pp. 151–160, 2019.

[28] M. Sundeep, S. Mahendran, T. Kannan Mahadevan, V. Kumar, and N. Parthipan, "Optimization of drilling parameters on austenitic stainless steel (AISI 316) using taguchi's methodology," *The International Journal of Robotics Research*, vol. 3, no. 4, p. 388, 2014.

[29] T. Das, A. Erdogan, B. Kursuncu, E. Maleki, and O. Unal, "Effect of severe vibratory peening on microstructural and

tribological properties of hot rolled AISI 1020 mild steel," *Surface and Coatings Technology*, vol. 403, 2020.

[30] M. Nouari, G. List, F. Girot, and D. Géhin, "Effect of machining parameters and coating on wear mechanisms in dry drilling of aluminium alloys," *International Journal of Machine Tools and Manufacture*, vol. 45, no. 12-13, pp. 1436–1442, 2005.

[31] H. A. Youssef and H. El-Hofy, *Machining Technology: Machine Tools and Operations*, CRC Press, Boca Raton, FL, USA, 2008.

[32] M. Nouari, G. List, F. Girot, and D. Coupard, "Experimental analysis and optimisation of tool wear in dry machining of aluminium alloys," *Wear*, vol. 255, no. 7-12, pp. 1359–1368, 2003.

[33] M. Balaji, K. Venkata Rao, N. Mohan Rao, and B. S. N. Murthy, "Optimization of drilling parameters for drilling of TI-6Al-4V based on surface roughness, flank wear and drill vibration," *Measurement*, vol. 114, pp. 332–339, 2018.

[34] B. M. Gopalsamy, B. Mondal, and S. Ghosh, "Taguchi method and ANOVA: an approach for process parameters optimization ofhard machining while machining hardened steel," *Journal of Scientific and Industrial Research*, vol. 68, 2009.

[35] G. R. Johnson and W. H. Cook, "Fracture characteristics of three metals subjected to various strains, strain rates, temperatures and pressures," *Engineering Fracture Mechanics*, vol. 21, no. 1, pp. 31–48, 1985.

[36] M. N. A. Nasr, *On modelling of machining-induced residual stresses*, Ph.D. thesis, McMaster University, Hamilton, ON, Canada, 2008.

[37] D. Zhu, X. Zhang, and H. Ding, "Tool wear characteristics in machining of nickel-based superalloys," *International Journal of Machine Tools and Manufacture*, vol. 64, pp. 60–77, 2013.

[38] K. Carter-Journet, A. Kale, D. Zhang, E. Pradeep, T. Falgout, and L. Heuermann-Kuehn, "Estimating probability of failure for drilling tools with life prediction," in *Proceedings of the SPE Asia Pacific Oil and Gas Conference and Exhibition*, Adelaide, Australia, October 2014.

[39] M. Sarıkaya, M. K. Gupta, I. Tomaz et al., "A state-of-the-art review on tool wear and surface integrity characteristics in machining of superalloys," *CIRP Journal of Manufacturing Science and Technology*, vol. 35, pp. 624–658, 2021.

[40] P. F. Zhang, N. J. Churi, Z. J. Pei, and C. Treadwell, "Mechanical drilling processes for titanium alloys: a literature review," *Machining Science and Technology*, vol. 12, no. 4, pp. 417–444, 2008.

[41] J. Xu, A. Mkaddem, and M. El Mansori, "Recent advances in drilling hybrid FRP/Ti composite: a state-of-the-art review," *Composite Structures*, vol. 135, pp. 316–338, 2016.

[42] J. Y. Sheikh-Ahmad, "Nontraditional machining of FRPs," in *Machining of Polymer Composites*, pp. 237–291, Springer, Cham, 2009.

[43] R. Tyagi, "Processing techniques and tribological behavior of composite materials," *IGI Global*, 2015.

[44] P. F. Zhang, N. J. Churi, Z. J. Pei, and C. Treadwell, "Mechanical drilling processes for titanium alloys: a literature review," *Machining Science and Technology*, vol. 12, no. 4, pp. 417–444, 2008.

[45] S. Sharif, E. Abd, and H. Sasahar, "Machinability of titanium alloys in drilling," *Titanium Alloys-Towards Achieving Enhanced Properties for Diversified Applications*, vol. 3, pp. 117–137, 2012.

[46] M. Aamir, M. Tolouei-Rad, K. Giasin, and A. Nosrati, "Recent advances in drilling of carbon fiber–reinforced polymers for aerospace applications: a review," *The International Journal of Advanced Manufacturing Technology*, vol. 105, no. 5-6, pp. 2289–2308, 2019.

[47] S. Vigneshwaran, M. Uthayakumar, and V. Arumugaprabu, "Review on machinability of fiber reinforced polymers: a drilling approach," *Silicon*, vol. 10, no. 5, pp. 2295–2305, 2018.

[48] N. Uçak and A. Çiçek, "The effects of cutting conditions on cutting temperature and hole quality in drilling of Inconel 718 using solid carbide drills," *Journal of Manufacturing Processes*, vol. 31, pp. 662–673, 2018.

[49] S. Karabulut, "Study on machining parameters for thrust force and torque in milling aa7039 composites reinforced with al2o3/b4c/sic particles," *International Journal of Engineering Technologies IJET*, vol. 2, no. 2, pp. 68–75, 2016.

[50] Y. Kaplan, Ş. Okay, R. M. Ali, and M. Nalbant, "Investigation of the effects of machining parameters on the thrust force and cutting torque in the drilling of AISI D2 and AISI D3 cold work tool steels," 2014, https://nopr.niscpr.res.in/bitstream/123456789/28779/3/IJEMS%2021(2)%20128-138.pdf.

[51] X. Liu, R. DeVor, and S. Kapoor, "An analytical model for the prediction of minimum chip thickness in micromachining," *Journal of Manufacturing Science and Engineering*, vol. 148, 2006.

[52] R. V. S. Singh, B. Latha, and V. Senthilkumar, "Modeling and analysis of thrust force and torque in drilling GFRP composites by multi-facet drill using fuzzy logic," *International Journal of Recent Trends in Engineering*, vol. 1, no. 5, p. 66, 2009.

[53] C. S. Akhil, M. H. Ananthavishnu, C. K. Akhil, P. M. Afeez, R. Akhilesh, and R. Rajan, "Measurement of cutting temperature during machining," *IOSR Journal of Mechanical and Civil Engineering*, vol. 13, no. 2, pp. 108–122, 2016.

[54] M. Uddin, A. Basak, A. Pramanik, S. Singh, G. M. Krolczyk, and C. Prakash, "Evaluating hole quality in drilling of Al 6061 alloys," *Materials*, vol. 11, no. 12, p. 2443, 2018.

[55] R. A. Gonçalves and M. B. d. Silva, "Influence of copper content on 6351 aluminum alloy machinability," *Procedia Manufacturing*, vol. 1, pp. 683–695, 2015.

[56] G. Samy and S. T. Kumaran, "Measurement and analysis of temperature, thrust force and surface roughness in drilling of AA (6351)-B4C composite," *Measurement*, vol. 103, pp. 1–9, 2017.

[57] W. Chen, "Cutting forces and surface finish when machining medium hardness steel using CBN tools," *International Journal of Machine Tools and Manufacture*, vol. 40, no. 3, pp. 455–466, 2000.

[58] M. Boopathi, S. Shankar, S. Manikandakumar, and R. Ramesh, "Experimental investigation of friction drilling on brass, aluminium and stainless steel," *Procedia Engineering*, vol. 64, pp. 1219–1226, 2013.

[59] C. E. Bates, "Study examines influences on machinability of iron castings," *Modern Casting*, vol. 86, no. 10, pp. 36–39, 1996.

[60] J. Zang, J. Zhao, A. Li, and J. Pang, "Serrated chip formation mechanism analysis for machining of titanium alloy Ti-6Al-4V based on thermal property," *The International Journal of Advanced Manufacturing Technology*, vol. 98, no. 1-4, pp. 119–127, 2018.

[61] H. Yanda, J. A. Ghani, M. N. A. M. Rodzi, K. Othman, and C. H. Che Haron, "Optimization of material removal rate, surface roughness and tool life on conventional dry turning of FCD700," *International Journal of Mechanical and Materials Engineering*, vol. 5, no. 2, pp. 182–190, 2010.

[62] J. Z. Zhang and J. C. Chen, "Surface roughness optimization in a drilling operation using the Taguchi design method," *Materials and Manufacturing Processes*, vol. 24, no. 4, pp. 459–467, 2009.
[63] M. Ratnam, "Factors affecting surface roughness in finish turning," *Comprehensive Materials Finishing*, vol. 1, 2017.
[64] K. Giasin, S. Ayvar-Soberanis, and A. Hodzic, "An experimental study on drilling of unidirectional GLARE fibre metal laminates," *Composite Structures*, vol. 133, pp. 794–808, 2015.
[65] A. Olabi and M. Hashmi, "Stress relief procedures for low carbon steel (1020) welded components," *Journal of Materials Processing Technology*, vol. 56, no. 1-4, pp. 552–562, 1996.
[66] S. P. Dwivedi, S. Kumar, and A. Kumar, "Effect of turning parameters on surface roughness of A356/5% SiC composite produced by electromagnetic stir casting," *Journal of Mechanical Science and Technology*, vol. 26, no. 12, pp. 3973–3979, 2012.
[67] K. Giasin, S. Ayvar-Soberanis, T. French, and V. Phadnis, "3D finite element modelling of cutting forces in drilling fibre metal laminates and experimental hole quality analysis," *Applied Composite Materials*, vol. 24, no. 1, pp. 113–137, 2017.
[68] M. Kurt, Y. Kaynak, and E. J. T. I. J. o.A. M. T. Bagci, "Evaluation of drilled hole quality in Al 2024 alloy," *The International Journal of Advanced Manufacturing Technology*, vol. 37, no. 11-12, pp. 1051–1060, 2008.
[69] C. Çakır, *Principles of Modern Machining*, Nobel Publishing, Ankara, 2006.
[70] E. Trent and P. J. H. Wright, *Metal Cutting*, Butherworth, Oxford, UK, 1991.
[71] S. Qu, F. Sun, L. Zhang, and X. Li, "Effects of cutting parameters on dry cutting of aluminum bronze alloy," *The International Journal of Advanced Manufacturing Technology*, vol. 70, no. 1-4, pp. 669–678, 2014.
[72] E. Yarar, A. T. Ertürk, F. G. Koç, and F. Vatansever, "Comparative analysis in drilling performance of AA7075 in different temper conditions," *Journal of Materials Engineering and Performance*, vol. 32, no. 17, pp. 7721–7736, 2023.
[73] A. T. Ertürk, E. Yarar, G. Özer, and M. E. Bulduk, "Post-process drilling of AlSi10Mg parts by laser powder bed fusion," *The International Journal of Advanced Manufacturing Technology*, vol. 126, no. 3-4, pp. 1199–1212, 2023.
[74] H. K. Toenshoff and B. Denkena, *Basics of Cutting and Abrasive Processes*, Springer, Cham, 2013.
[75] M. P. Groover, *Fundamentals of Modern Manufacturing: Materials, Processes, and Systems*, John Wiley and Sons, Hoboken, NJ, USA, 2020.
[76] K. Liu, J. Li, J. Sun, Z. Zhu, and H. Meng, "Investigation on chip morphology and properties in drilling aluminum and titanium stack with double cone drill," *The International Journal of Advanced Manufacturing Technology*, vol. 94, no. 5-8, pp. 1947–1956, 2018.
[77] M. SenthilKumar, A. Prabukarthi, and V. J. P. e. Krishnaraj, "Study on tool wear and chip formation during drilling carbon fiber reinforced polymer (CFRP)/titanium alloy (Ti6Al4 V) stacks," *Procedia Engineering*, vol. 64, pp. 582–592, 2013.
[78] J. Sun and Y. Guo, "A new multi-view approach to characterize 3D chip morphology and properties in end milling titanium Ti–6Al–4V," *International Journal of Machine Tools and Manufacture*, vol. 48, no. 12-13, pp. 1486–1494, 2008.
[79] Z. Zhu, K. Guo, J. Sun et al., "Evolution of 3D chip morphology and phase transformation in dry drilling Ti6Al4V alloys," *Journal of Manufacturing Processes*, vol. 34, pp. 531–539, 2018.